

Article

Characteristics of Vibration Velocity Signal Using Liquid Carbon Dioxide Rock-Breaking Technology

Chong Yu ^{1,*}, Xiaohu Wang ^{1,2}, Jiajun Wu ^{1,2} and Yongan Ma ^{1,2}

¹ State Key Laboratory of Geomechanics and Geotechnical Engineering, Institute of Rock and Soil Mechanics, Chinese Academy of Sciences, Wuhan 430071, China; wangxiaohu201@mails.ucas.ac.cn (X.W.)

² University of Chinese Academy of Sciences, Beijing 100049, China

* Correspondence: cyu@whrsm.ac.cn

Abstract: Liquid carbon dioxide rock-breaking (L-CDRB) is a new physical blasting technology. To study the characteristics of its vibration velocity, rock-breaking field tests were conducted using a new type of liquid CO₂ fracturing tube. Comparisons were made between explosive blasting and L-CDRB in terms of the peak values, frequencies, and energy distributions of the generated vibration velocities. The results show that (1) for the same scaled charge, L-CDRB (vs. explosive blasting) produced a smaller peak, a lower dominant frequency, and simpler frequency components of vibration velocities than explosive blasting. (2) The dominant frequency and energy distribution were related to the total liquid CO₂ filling quantity. Higher total filling quantities resulted in higher dominant frequencies, and the energy distribution shifted from a low to a high-frequency band.

Keywords: CO₂ rock-breaking; scaled charge; attenuation law; frequency domain analysis

1. Introduction

Dynamic loads can be generated during blasting, causing the rock mass to crack quickly [1]. Therefore, this technique is widely utilized in some engineering construction fields, such as mining, tunneling, and nuclear power plant construction. However, blasting construction can also cause secondary hazards—including blasting dust, polluted gas, flying rock, noise, shock waves, and vibrations—the last of which is the primary hazard and an important factor in blasting design. Blasting vibration velocities are strictly regulated [2], especially when the blasting area is close to buildings, installations, and other specially protected objects. Traditional non-explosive methods, such as demolition agents and rock-breaking machines, are generally time-consuming. In addition, hydraulic fracturing (HF) is also an increasingly popular method [3], which can better control the direction of crack development. However, it is worth noting that HF technology is commonly used in the development of oil and gas wells and is relatively expensive. Liquid carbon dioxide rock-breaking (L-CDRB) technology considering both rock-breaking efficiency and economic cost [4,5], at the same time, produces a much smaller vibration velocity and has a wide range of applications in special situations in which vibration velocities are severely limited.

CO₂ phase transition blasting technology was first introduced by the British company Cardox and was called the Cardox tube system. In the early 1960s, this nontraditional physical blasting technology began to be used in Europe and the United States [3,4]. S.P. Singh introduced the structure and use of the device earlier, noting that the Cardox device could be used for large-scale quarry excavations and demolition blasting for concrete structures [5]. Earlier, Turkey applied L-CDRB to coal mining to increase the lump coal output [6].

The current research on this technology is focused on the fracturing mechanism, engineering applications, and equipment improvements. Guo [7] studied the process of L-CDRB and noted that the technology could be used to blast brittle, porous materials, and the single-release power is influenced by the peak pressure and the liquid CO₂ volume.



Citation: Yu, C.; Wang, X.; Wu, J.; Ma, Y. Characteristics of Vibration Velocity Signal Using Liquid Carbon Dioxide Rock-Breaking Technology. *Appl. Sci.* **2023**, *13*, 4285. <https://doi.org/10.3390/app13074285>

Academic Editor: Giuseppe Lacidogna

Received: 22 February 2023

Revised: 23 March 2023

Accepted: 24 March 2023

Published: 28 March 2023



Copyright: © 2023 by the authors. Licensee MDPI, Basel, Switzerland. This article is an open access article distributed under the terms and conditions of the Creative Commons Attribution (CC BY) license (<https://creativecommons.org/licenses/by/4.0/>).

Xu and Cheng [8,9] developed a high-pressure gas-blasting simulation testing system to research the mechanism of L-CDRB. Zhou [10] established a finite difference constitutive model based on the theory of damage mechanics and aerodynamics to calculate the effective influence radius of liquid CO₂ single-hole blasting. Xiao [11] carried out multiple groups of tests by changing the liquid CO₂ filling amount, the rated pressure of the constant pressure rupture disc, and the combustion agent amounts. The author also measured the pressure change law in the fracturing tube and concluded that the tube's energy was mainly related to the rated pressure of the constant pressure rupture disc and that the energy utilization rate could be improved by increasing the disc's rated pressure. In engineering applications, Tsuyoshi [12] and Niezgodá [13] found that CO₂ anti-permeability technology was superior to hydraulic fracturing through testing and numerical simulation, respectively. Han [14] noted the difference between this technology's applications in the fields of coal seam permeability enhancement and rock-breaking. Su [15] carried out four L-CDRB tests under different geological conditions in an open-air site and noted that the L-CDRB capacity was closely related to the site's geological conditions, hole arrangement, and other design parameters. Xia [16] noted that the technology has a good blasting vibration reduction effect by field testing L-CDRB in the excavation site of the foundation pit of a nuclear power plant.

Rock-like brittle materials exhibit different mechanical characteristics under static and dynamic loading conditions [17,18]. The deformation characteristics, failure strength, and fracture characteristics of rocks at high strain rates are all affected by rate effects. According to different loading rates, rock strain rate characteristics can be classified from low to high into creep, quasi-static loading, medium strain rate, high strain rate, and ultra-high strain rate [19]. Under impact and explosion loads, rocks are subjected to large impact loads in a short period of time, and their stress characteristics fall within the range of ultra-high strain rates and high strain rates. Carbon dioxide phase change blasting has a much smaller loading stress peak and pressure boosting time than explosive blasting. According to current research, three commonly used rock-breaking techniques can be used: explosive blasting, L-CDRB, and HF. The pressure-loading characteristics of different rock-breaking methods are listed in Table 1.

Table 1. Loading parameters of different rock-breaking techniques.

Technology	Peak Pressure (MPa)	Time of Pressure Rise (s)	Pressure Duration (s)
Explosive	$>10^4$	10^{-7}	10^{-6}
L-CDRB	10^2	10^{-3}	10^{-2}
HF	10	10^2	10^4

The rock-breaking process of L-CDRB technology is divided into two parts. The first part is the impact of high-pressure carbon dioxide on the rock mass, and the second part is the quasi-static carbon dioxide driving the further development of cracks. Gao [20] obtained a formula for calculating the radius of the fracture zone by analyzing the process of rock cracking caused by carbon dioxide phase transformation and pointed out that the effect of rock breaking can be improved by increasing the initial pressure of liquid carbon dioxide in the fracturing tube. Through model tests, Zhang [21] found that carbon dioxide does not produce a fracture zone in rock breaking, and stress waves are the main cause of damage to concrete model specimens. The structure of the cracking tube has an important impact on the rock-breaking effect.

As this technology has been applied in various engineering projects, some scholars have studied a new type of fracturing tube, which changes the way pressure is released from the tube's end to its lateral side. Thus, the pressure acts more evenly on the blast hole, minimizing accidents resulting from the first-generation fracturing tube being stuck or blown off in practical applications. Zhu [22] and Li [23] studied the equivalent energy and characteristics of the blasting vibration signals of the new type of fracturing tube and noted its greater safety and efficiency. At present, no reports directly monitor the internal

pressure of the new type of fracturing tube, and few comparative test studies have been made on L-CDRB and explosive blasting in the same field.

In this study, the vibration propagation law of the CO₂ rock-breaking technology was investigated by carrying out field tests in an open pit mine, and the main innovations are as follows. (1) Large-scale field trials were carried out using 1378 kg of liquid CO₂. (2) The new fracturing tube was used, and the pressure relief method was changed from the tube's end to its lateral side. (3) At the same site, a monitoring comparison was conducted on the vibration velocities between explosive blasting and L-CDRB, and the characteristics of the low vibration velocities produced by L-CDRB are described here in detail. (4) A wide range of vibration monitoring tests were conducted with many pieces of vibration velocity monitoring equipment arranged at different distances (9.7–260.5 m) from the explosion zone's center, so the vibration velocity attenuation law obtained here is more reliable.

2. Field Test

2.1. New CO₂ Rock-Breaking System

This test used a CPD-ZLG series fracturing tube. The fracturing tube was 89 mm in diameter and 1200 mm in length. Its main material was high-quality No. 2 carbon steel with a wall thickness of 4 mm. L-CDRB system is shown in Figure 1. A high-pressure pulse initiator was used to trigger the activator reaction inside the fracturing tube, providing high-temperature conditions under which liquid CO₂ can be rapidly vaporized. Different from the first generation of fracturing tubes, this type of fracturing tube eliminates the design of a constant pressure shear plate and energy relief head by instantaneous vaporizing liquid CO₂ to produce high pressure that tears the tube's wall, so the pressure acts more evenly in the blast hole.

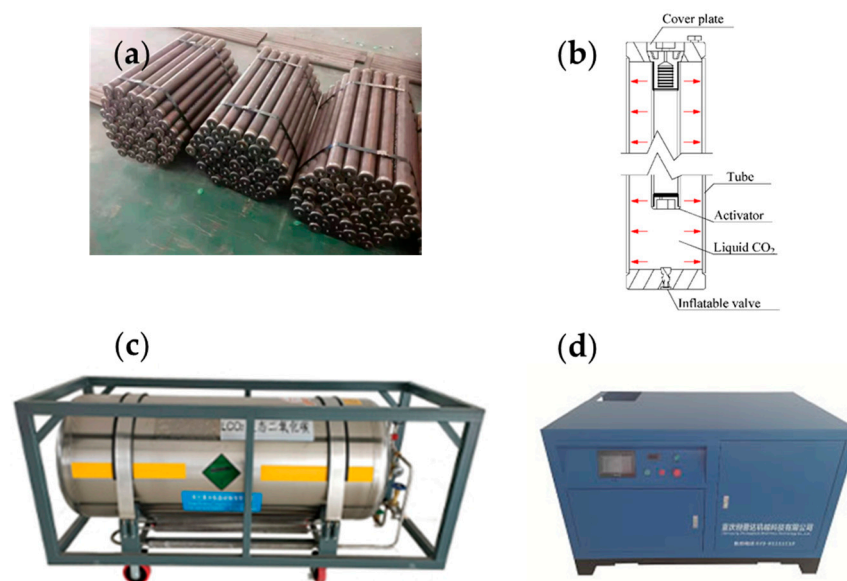


Figure 1. L-CDRB system: (a) fracturing tube; (b) tube's construction; (c) liquid carbon dioxide storage equipment; (d) filling machine.

2.2. Test Parameters

The experiment was conducted in an open pit mine in Panzhihua City, Sichuan Province. In order to understand the basic mechanical properties of rock mass in the rock-breaking area, we conducted core sampling on-site, processed the core into standard test pieces with a diameter of 50 mm and a length of 100 mm in accordance with relevant specifications [24], and conducted uniaxial compression tests using the RMT-150C testing machine (Figure 2).

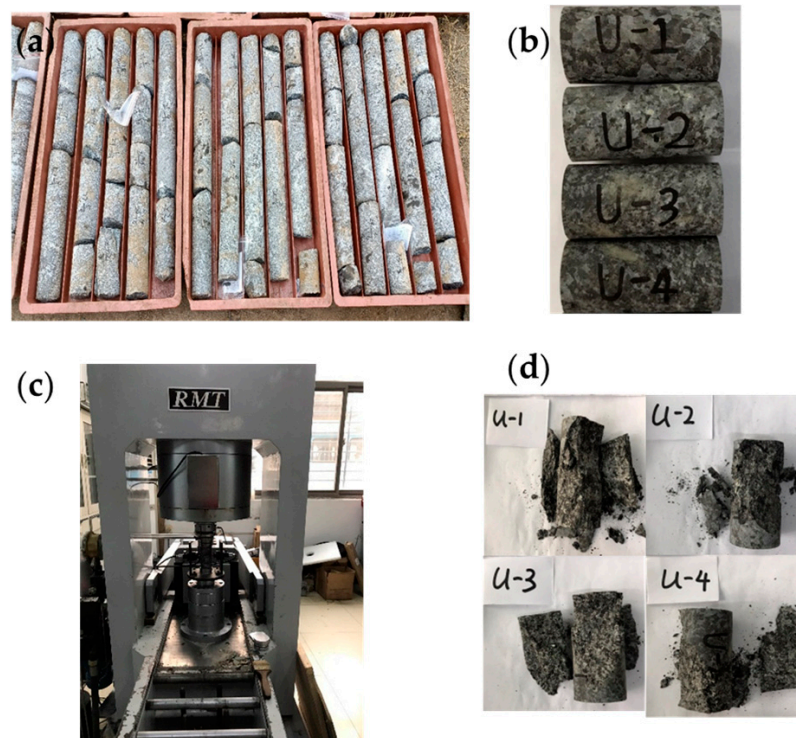


Figure 2. Uniaxial compression test: (a) field coring; (b) test piece; (c) RMT-150C; (d) damaged test piece (Test piece No.: U-1~U-4).

The stress–strain curve of the uniaxial compression test is shown in Figure 3, and the test results are summarized in Table 2. Rock mechanics tests showed that the average uniaxial compressive strength of the rocks in this area was 114.43 MPa, the tangent modulus of elasticity was 52.14 GPa, and the Poisson’s ratio was 0.31.

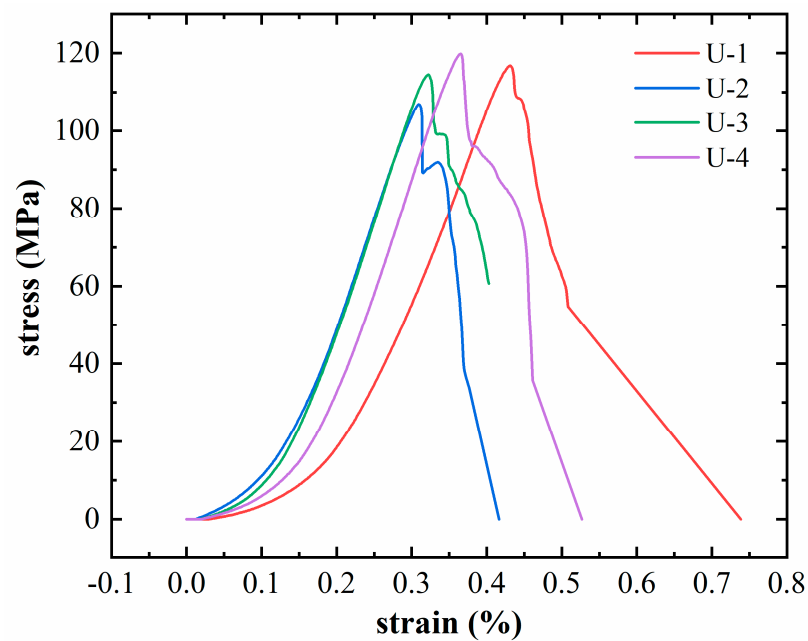


Figure 3. Stress-strain curve of uniaxial compression test.

Table 2. Statistics of uniaxial compression test results.

Test No.	Uniaxial Strength (MPa)	Elastic Modulus (GPa)	Poisson's Ratio
U-1	116.70	44.83	0.51
U-2	106.80	53.22	0.34
U-3	114.41	55.59	0.11
U-4	119.79	54.93	0.27
Average	114.43	52.14	0.31

The L-CDRB tests were conducted three times. The first test was designed as a single-row hole, and the second and third were double-row holes with plum-shaped layouts with a hole spacing of 1 m and a row spacing of 0.7 m, See Table 3 for specific parameters. In addition, blast vibration monitoring was conducted three consecutive times for explosives at the same test site, the design parameters for which are shown in Table 4.

Table 3. L-CDRB test parameters.

Test No.	No. of Holes	No. of Tubes	Fill Pressure (MPa)	Fill Quantity (kg)	Hole Depth (m)
01	8	40	8	208	16.5
02	13	97	8	504.4	16.5
03	21	128	8	665.6	16.5

Table 4. Explosive blasting test parameters.

Test No.	No. of Holes	Hole Depth (m)	Total Charge (kg)	Segmented Charge (kg)	Consumption (kg/m ³)
04	58	16.8	15,070	280	0.71
05	49	17.0	12,880	280	0.61
06	101	14.4	11,945	300	0.68

2.3. Monitoring Program

Both pressure and blasting vibration were monitored. For the L-CDRB tests, the fracturing tube bore pressure and the blast vibration velocity were monitored. For the explosive tests, the blast vibration velocity was monitored.

The pressure testing system is mainly composed of a pressure sensor, a multi-functional collector, and control software. The connection method is shown in Figure 4a. In order to obtain a complete internal pressure curve of the cracking tube, we machined a threaded hole of suitable sensor size on the top of the fracturing tube and fixed the sensor to the end of the fracturing tube; as shown in Figure 4b, the pressure sensor was a KD2000 series large-range piezoelectric sensor. The pressure-sensing part of the sensor is located inside the tube. Then, the data are transmitted to the acquisition instrument through a data line, and finally, the pressure signal is recorded and stored by the acquisition software.

In this test, a TC4850 self-registering instrument monitoring system was used to record the vibration velocity in three directions: vertical, horizontal-radial, and horizontal-tangential. When the monitoring points were placed, the sensors were fixed to the intact bedrock surface by using quick-setting plaster, with the X direction being that of the blast zone (see Figure 5). Three to seven pieces of monitoring equipment were placed for each test, depending on the site's actual geological conditions, and the equipment was distributed within 9.7–260.5 m from the center of the blast zone to ensure that adequate vibration data were obtained.



Figure 4. Pressure test system: (a) composition and connection mode of pressure test system; (b) installation of sensors.

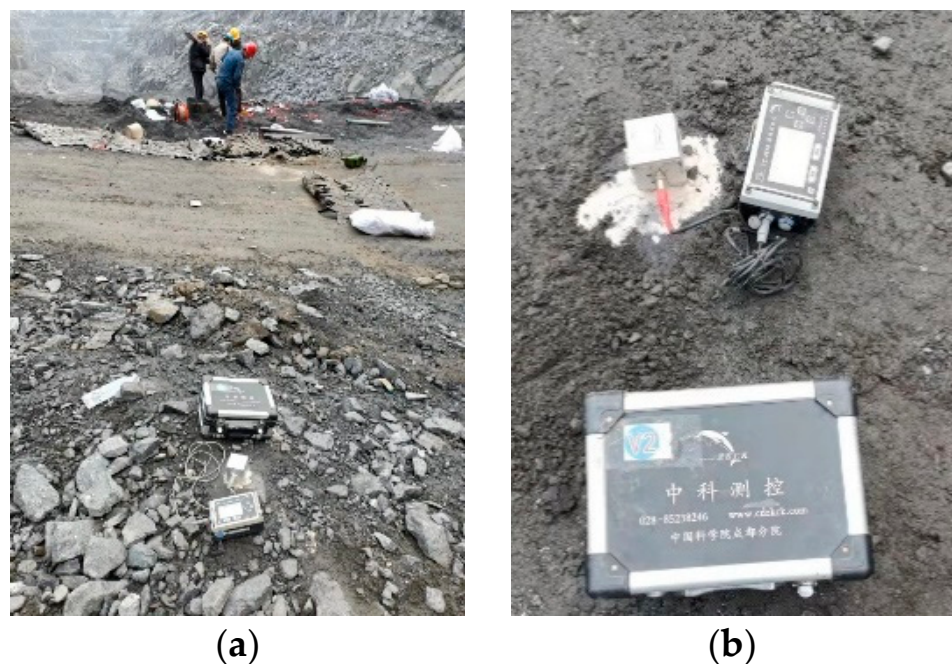


Figure 5. Vibration velocity monitoring equipment. (a) Relative position of velocity sensor and rock breaking area; (b) Installation diagram of speed sensor.

3. Test Results

The three L-CDRB field tests resulted in no engineering accidents such as stuck, flying, or unexploded tubes, which greatly improved the safety of the field construction compared to the first generation of fracturing tubes. The fracturing tubes can be filled, deployed, and detonated in a series of processes with only two people working together, which greatly improves construction efficiency.

3.1. Rock Breaking Effect

Blast pile fragmentation analysis is commonly used to evaluate the effect of rock fragmentation by blasting. Therefore, we used the method of image analysis to compare and evaluate the fragmentation of explosive blasting and L-CDRB technology, as shown in Figure 6. The fragmentation of L-CDRB is greater than that of explosive blasting, D_{50} of L-CDRB is 1009.03 mm, explosive's $D_{50} = 735.95$ mm (D_{50} : dimensions less than 50% of the total material).

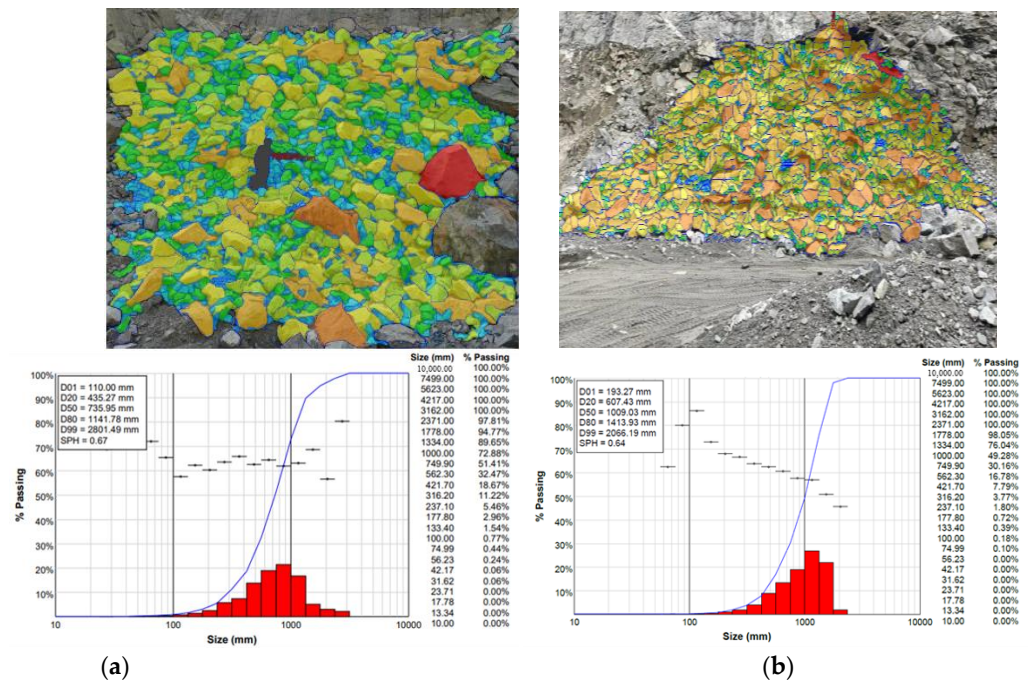


Figure 6. Fragment-size distribution: (a) explosive; (b) L-CDRB.

3.2. Pressure Test Results

Figure 7 shows the p–t curve inside the fracturing tube, which can be divided into four stages. The first stage is the pressure increase stage, in which the pressure pulse current excites the activator to produce a chemical reaction, generating a large amount of high-temperature gas. Liquid CO₂ absorbs heat and instantly vaporizes and expands, so the pressure inside the fracturing tube increases rapidly, reaching a peak of 180.2 MPa in approximately 60 μs. In the second stage, the pressure inside the fracturing tube decreases rapidly to a negative state due to the overall tearing of the fracture tube wall. In the third stage, the pressure continues to increase to a second peak of approximately 90 MPa, as the liquid CO₂ does not completely vaporize at the time that the fracturing tube ruptures. The fourth stage is the oscillation stage, in which the gaseous CO₂ interacts with the fracturing tube wall to produce a partially reflected airflow, which interacts with the subsequently vaporized CO₂. This interaction results in a pressure oscillation that continues until the liquid CO₂ is completely vaporized, at which point the pressure returns to normal atmospheric pressure. The entire pressure relief process lasts approximately 140 μs.

3.3. Equivalent Energy Conversion

In quantification of the energy generated during L-CDRB, the commonly used method is to convert the breaking power into a TNT equivalent [25–27], which is of guiding significance for quantifying the practical application of liquid CO₂ phase change breaking capability.

Before the phase change of liquid CO₂ breaks the rock, the CO₂ in the fracturing tube coexists in a gas-liquid phase. After the phase change, the gas-liquid phase CO₂ in the fracturing tube is rapidly transformed into the gaseous state. The process can be calculated by compressed gas and water vapor vessel-blasting theory. The equation can be expressed as follows:

$$E_g = \frac{pV}{K_0 - 1} \left[1 - \left(\frac{0.1013}{p} \right)^{\frac{K_0 - 1}{K_0}} \right] \times 10^3 \quad (1)$$

where E_g is the gas blast energy, measured in kJ; p is the absolute ultimate pressure of the gas in the tube, measured in MPa; V is the volume of the vessel, measured in m³; and K_0 is

the adiabatic index of gas, i.e., the ratio of the constant pressure specific heat capacity to the constant volume specific heat capacity of CO₂, measured as $K_0 = 1.295$.

The energy of the CPD-ZLG fracture tube used in this test was calculated to be 3013.4 kJ. The TNT equivalent was calculated from Equation (2):

$$W_{TNT} = \frac{E_g}{Q_{TNT}} \tag{2}$$

where $Q_{TNT} = 4250$ kJ and $E_g = 3089.17$ kJ. The equation gives $W_{TNT} = 0.727$ kg. The energy of 1 kg of No. 2 rock emulsion explosive is 3009 kJ, and the energy of a single fracture tube is equivalent to 1.024 kg of No. 2 rock emulsion explosive.

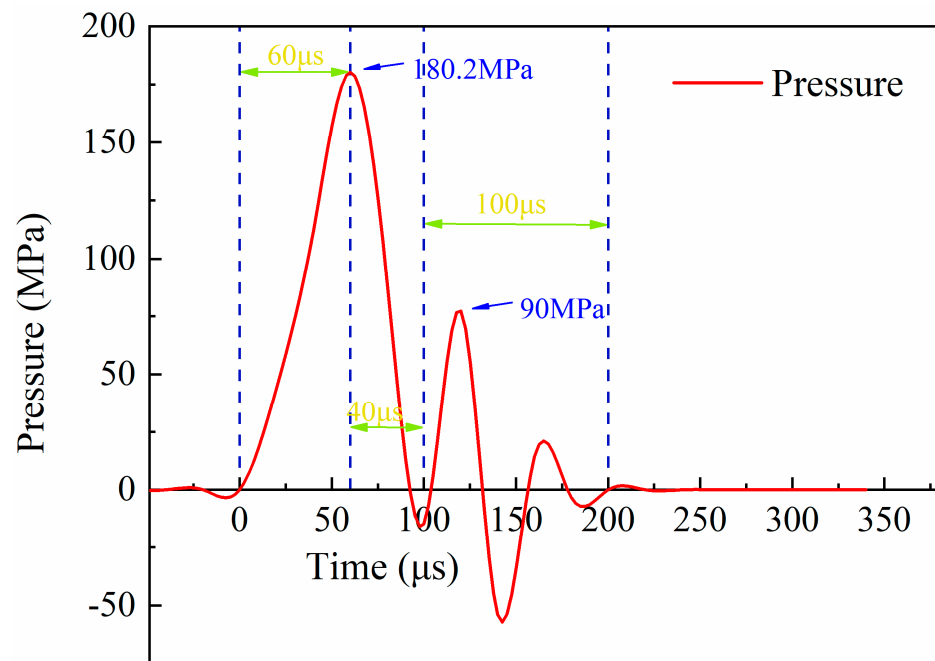


Figure 7. Fracturing tube’s internal p-t curve.

3.4. Vibration Velocity Monitoring Results

3.4.1. Vibration Velocity Peak Analysis

Blast design is intended to attenuate blasting vibrations [28,29], and the blasting vibration attenuation law is closely related to the explosive type as well as the propagation site. This experiment uses Sadov’s formula to analyze the vibration attenuation law:

$$PPV = K(Q^{1/3}R)^\alpha \tag{3}$$

where PPV (peak particle velocity) is measured in cm/s; Q is the explosive quantity (kg), which is the total charge in the simultaneous blasting and the maximum section charge in the delay blasting; R is the distance of explosion source, which indicates the distance between the monitoring point and the blasting point (m); $Q^{1/3}/R$ is the scaled charge; and K and α are the coefficients and attenuation indices related to the topography and geological conditions from the blasting to the monitoring point, respectively. As α increases, the blasting vibration is attenuated more rapidly.

At present, there is no empirical formula for the vibration velocity attenuation law of L-CDRB. For a comparative analysis, the mass of a single charge of liquid CO₂ is converted into an equivalent emulsion explosive mass of equal energy, Q_t , with reference to Sadov’s formula. Based on the data obtained from the field test monitoring, the nonlinear data were fitted, as shown in Figure 8.

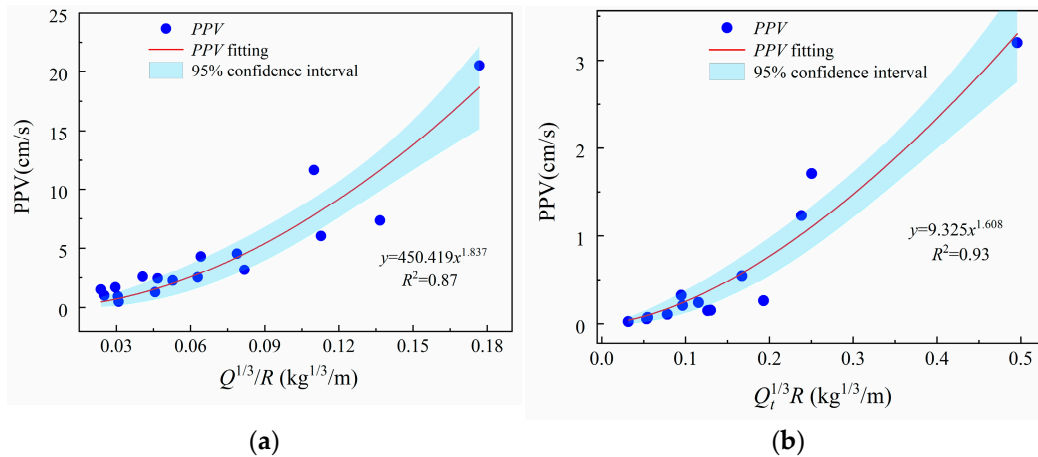


Figure 8. Vibration velocity attenuation law: (a) explosive blasting; (b) L-CDRB.

The explosive blasting and L-CDRB vibration velocity attenuation laws are stated in Equations (4) and (5):

$$PPV_{ex} = 450.419(Q^{1/3}/R)^{1.837} \tag{4}$$

$$PPV_{CO2} = 9.450(Q_t^{1/3}/R)^{1.608} \tag{5}$$

A comparison of these two test methods reveals that the attenuation index of the explosive blasting vibration is $\alpha = 1.837$, and that of L-CDRB is $\alpha = 1.608$, which means the vibration attenuation rate of L-CDRB under the same site conditions is less than that of explosive blasting.

The PPV ratio produced by the two blasting methods can be expressed by Equation (6):

$$PPV_{ex}/PPV_{CO2} = 48.30(Q^{1/3}/R)^{0.229} \tag{6}$$

Figure 9 shows that larger-scaled changes have larger ratios but gradually decreasing rates of increase. When the scaled charge was 0.1, the vibration velocity of explosive blasting was 28.5 times that of L-CDRB, and when the scaled charge was 0.2, the ratio was 33 times. This result shows that L-CDRB is obviously superior to explosive blasting in reducing the vibration velocity, especially in areas close to the blasting center.

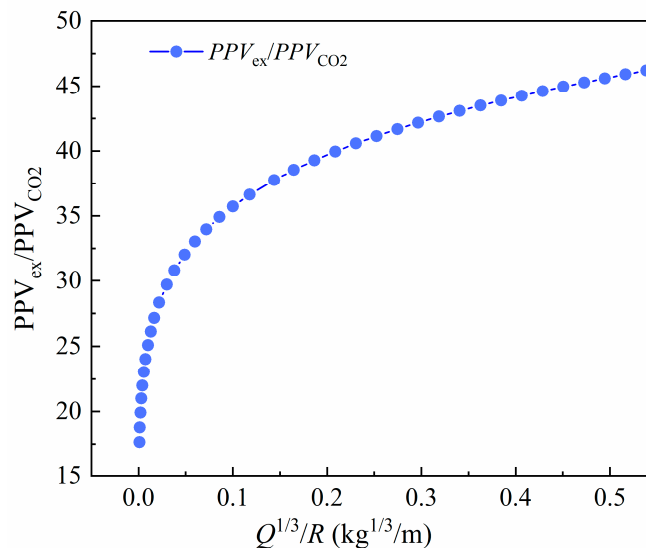


Figure 9. Peak particle velocity (PPV) comparison.

3.4.2. Frequency Domain Analysis

An analysis of the damage caused by blasting should consider not only the peak value of the vibration velocity but also the vibration signal’s frequency characteristics.

Fourier transform is often used in time–frequency domain signal conversion. Discrete time signal $x(n)$ can be converted to spectrum signal $X(j\omega)$ by a Fourier transform, and the conversion formula is:

$$X(j\omega) = \sum_{n=-\infty}^{\infty} x(n)e^{-j\omega n} \tag{7}$$

where j is an imaginary unit, and ω is the digital frequency.

Because blasting vibration signals have a limited length, the discrete Fourier transform is used in the actual processing. For vibration signal $x(n)$ with length n , the discrete Fourier transform formula is:

$$X(k) = \sum_{n=0}^{N-1} x(n)e^{-j(2\pi/N)kn} \tag{8}$$

where $X(k)$ ($k = 0, 1, 2, \dots, N - 1$) is the discrete Fourier coefficient, representing the amplitude of the corresponding frequency.

The main vibration frequency and frequency distribution characteristics of blasting vibrations can be analyzed by a discrete Fourier transform, and the energy distribution characteristics of the vibration signal in different frequency ranges can be further analyzed. The Fourier power spectrum can be calculated by Equation (9), and the cumulative power of the vibration signal can be calculated according to Equation (10).

$$P_k = X_k \overline{X_k} \tag{9}$$

$$C_m = \frac{\sum_{k=0}^m X_k}{\sum_{k=0}^{N-1} X_k} \tag{10}$$

where $\overline{X_k}$ is the conjugate complex numbers of Fourier coefficient X_k , $m = (1, 2, \dots, N - 1)$.

First, we compared the differences in the frequency domains of the vibration velocity signals generated by explosive blasting and L-CDRB. By using the scaled charge of the explosive method and the equivalent scaled charge of the L-CDRB method, monitoring points with approach equivalent scaled charges were selected for a Fourier spectrum analysis, as shown in Figure 10.

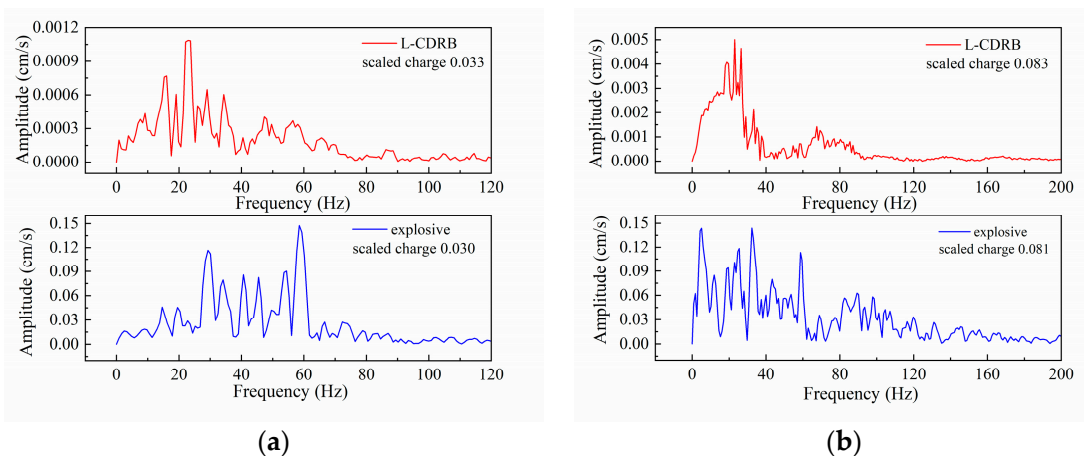


Figure 10. Frequency domain comparison of vibration velocities using different test methods: (a) scaled charge approach 0.03; (b) scaled charge approach 0.08.

Figure 10 shows that the dominant frequency of the explosive blasting vibration was higher, the frequency composition was richer, and the frequency range was wider. These results were related to the two tests' different detonation modes: explosive blasting for segmental detonation results in many interactions, such as superposition and reflection in the propagation process of the shock wave, meaning it has a more abundant frequency component. In L-CDRB, all the detonations occur at one time, so the frequency composition is relatively simple.

Figure 11 shows the energy accumulation of the vibration velocity signal in different frequency bands. When the equivalent scaled charge approaches 0.03 and 0.08, 60% of the energy of the L-CDRB vibration velocity signal was concentrated in the range of 10–30 Hz, and the explosive blasting was mainly concentrated in the range of 30–60 Hz. Thus, the energy of the vibration velocity signal generated by the L-CDRB was mainly concentrated in the lower frequency bands.

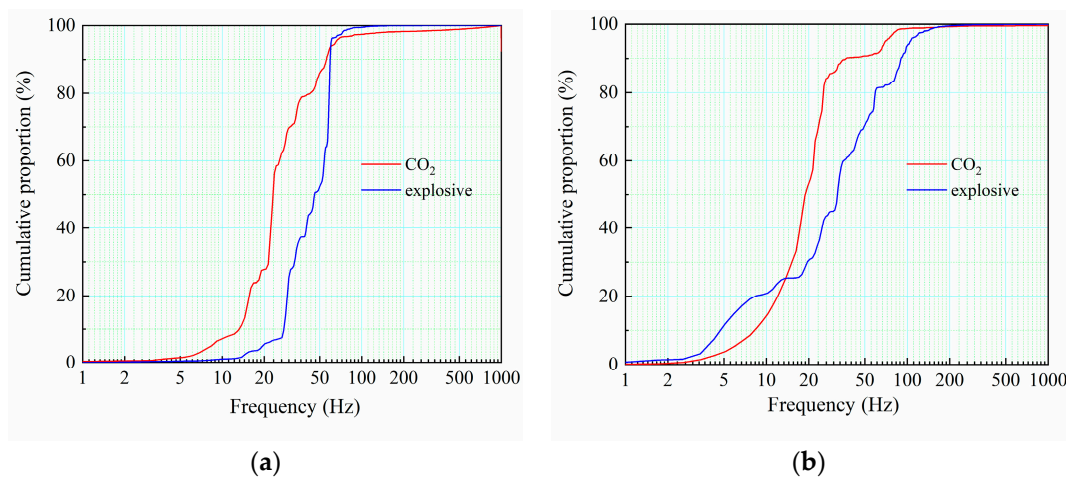


Figure 11. Energy distribution comparison of vibration velocities using different test methods: (a) scaled charge approach 0.03; (b) scaled charge approach 0.08.

To further analyze the frequency characteristics of the vibration signal generated by L-CDRB, monitoring points were selected in the three tests at the same distance from the explosion zone's center. Figure 12 shows that larger filling amounts of liquid CO₂ led to higher main frequencies of the vibration velocities, and the vibration energy gradually moved from a low to a high-frequency band.

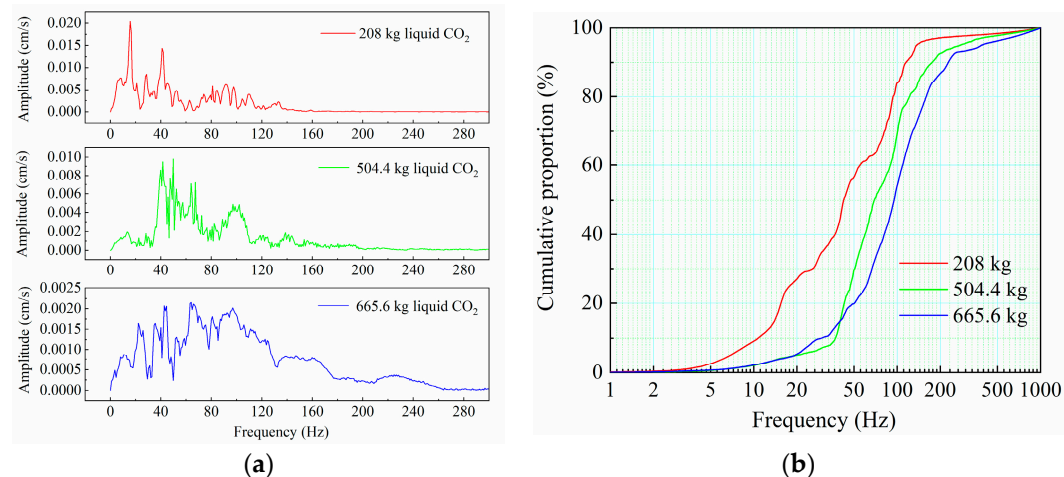


Figure 12. Comparison of vibration velocities under different filling amounts: (a) spectrum; (b) energy distribution.

4. Conclusions

This study conducted a field test of L-CDRB with a new type of fracturing tube, monitored the internal pressure of the fracturing tube and the site vibration velocity, and analyzed the characteristics of the vibration velocities produced by L-CDRB in comparison with explosive blasting at the same site. The main conclusions are as follows.

- (1) These tests resulted in no accidents, such as stuck, flying, or unexploded tubes or hole punches. This result indicates that this new type of fracturing tube is safer in engineering applications.
- (2) The pressure curve generated by the liquid CO₂ phase change in the fracturing tube was obtained, and the mass of liquid CO₂ was converted into the mass of explosives with the same energy using TNT equivalent as the medium. The calculation revealed that the energy of the CPD-ZLG fracturing tube was 3089.17 kJ, and a single fracturing tube was equivalent to 1.024 kg No. 2 rock emulsion explosive.
- (3) Based on energy equivalence, attenuation laws were for the vibration velocity of L-CDRB and explosive blasting. The former had a much lower vibration velocity than the latter. The PPV ratio of the two was related to the scaled charge. When the scaled charge was 0.1, the vibration velocity of explosive blasting was 28.5 times that of L-CDRB, and when the scaled charge was 0.2, the ratio was 33 times. This result fully illustrates that L-CDRB technology greatly reduces vibrations, especially in areas close to the blasting center.
- (4) Analyzed in detail here are the frequency domain characteristics of L-CDRB vibration velocities. The results show that compared with explosive blasting, L-CDRB has a lower dominant frequency of vibration velocities. From the perspective of energy distribution, approximately 60% of the energy is concentrated in the 10–30 Hz range, while explosive blasting produces vibration signal energy mainly concentrated in the 30–60 Hz range. The dominant frequency of vibration is related to the mass of liquid CO₂. As the total charge increases, the dominant frequency gradually increases, and the energy tends to move from a low to a high-frequency band.

5. Discussion

This study discusses the rock-breaking and vibration reduction effects of a new type of L-CDRB cracking tube. Field tests have demonstrated the safety and efficiency of this type of fracturing tube in use. By comparing the vibration speeds of explosive blasting at the same site, it quantitatively analyzes the vibration reduction effects of L-CDRB technology and discusses the factors that affect the main frequency of its vibration speed. These works are original and have not been carried out before. The further promotion and application of L-CDRB technology can be referred to as a good reference.

However, due to the limitations of actual conditions, the research work in this article has the following shortcomings. Currently, there are no relevant guidelines for the application of L-CDRB technology. This test was conducted in an open-pit mine, which is in a mining and production state. Therefore, the conduct of the test cannot affect the actual production work. Therefore, there are certain limitations in the setting of test parameters. Field tests with different pore network parameters should be continued to provide more reference basis for rock breaking under different conditions.

Author Contributions: Conceptualization, C.Y.; validation, J.W.; data curation, Y.M.; formal analysis, X.W. All authors have read and agreed to the published version of the manuscript.

Funding: This research was funded by the National Natural Science Foundation of China (No. U22A20239) and the National Key Research and Development Program of China (No. 2020YFA0711802).

Data Availability Statement: The data used to support the findings of this study are available within the article.

Conflicts of Interest: The authors declare no conflict of interest.

References

1. Liwang, L.; Haibo, L.; Xiaofeng, L. A state-of-the-art review of mechanical characteristics and cracking processes of pre-cracked rocks under quasi-static compression. *J. Rock. Mech. Geotech. Eng.* **2022**, *14*, 2034–2057.
2. GB 6722-2014; Safety Regulations for Blasting. AQSIQ: Beijing, China, 2014.
3. He, Q.; Zhu, L.; Li, Y.; Li, D.; Zhang, B. Simulating Hydraulic Fracture Re-orientation in Heterogeneous Rocks with an Improved Discrete Element Method. *Rock Mech. Rock Eng.* **2021**, *54*, 2859–2879. [[CrossRef](#)]
4. Kretzschmar, M.; Baira, E.M.; Uhlmann, E. Characterization of CO₂ snow generation to increase the blasting performance. *Appl. Mech. Mater.* **2015**, *794*, 255–261. [[CrossRef](#)]
5. Singh, S.P. Nonexplosive applications of the PCF concept for underground excavation. *Tunn. Undergr. Space Tech.* **1998**, *13*, 305–311. [[CrossRef](#)]
6. Holmberg, R.; White, T. Cardox system brings benefits in the mining of large coal. *Coal Intern.* **1995**, *243*, 27–28.
7. Zhixing, G. Liquid carbon dioxide blasting tube and field test. *Blast* **1994**, *3*, 72–74.
8. Ying, X. Development of high pressure gas blasting mining technology and its application in China. *Blasting* **1998**, *1*, 67–69.
9. Ying, X.; Yusheng, C. Model test study on coal breaking mechanism of high pressure gas blasting. *Coal Mine Blasting* **1996**, *3*, 1–4, 15.
10. Xihua, Z.; Jinlong, M.; Dongping, S.; Haibo, Z. Research on increasing coal seam permeability and promoting gas drainage with liquid CO₂ blasting. *Chin. Saf. Sci. J.* **2015**, *25*, 60–65.
11. Chengxu, X. *Experimental Study of Phase-Transforming Fracturing of Liquid Carbon Dioxide*; Hubei University of Technology: Wuhan, China, 2018; pp. 16–22.
12. Ishida, T.; Aoyagi, K.; Niwa, T.; Chen, Y.; Murata, S.; Chen, Q.; Nakayama, Y. Acoustic emission monitoring of hydraulic fracturing laboratory experiment with supercritical and liquid CO₂. *Geophys. Res. Lett.* **2012**, *39*, 16. [[CrossRef](#)]
13. Niezgoda, T.; Miedzinska, D.; Malek, E. Study on carbon dioxide thermodynamic behavior for the purpose of shale rock fracturing. *Bull. Pol. Acad. Sci.* **2013**, *3*, 605–612. [[CrossRef](#)]
14. Yabei, H. *Mechanism Research on Increase Coal Gas Permeability by Liquid CO₂ Phase Transition Fracturing Technique*; Henan Polytechnic University: Jiaozuo, China, 2014.
15. Kaikai, S. *Mechanism of Action and the Optimization of Construction Parameters of Opencast Mining of Rock with Carbon Dioxide Fracture*; Shandong University of Science and Technology: Qingdao, China, 2019.
16. Xiang, X.; Haibo, L.; Wang, X.; Zhou, Q.; Yu, C. Comparison analysis of ground vibrations induced by CO₂ gas fracturing and explosive blasting. *J. Rock. Mech. Eng.* **2021**, *40*, 1350–1356.
17. Hakalehto, K.O. Brittle fracture of rocks under impulse loads. *Int. J. Fract. Mech.* **1970**, *6*, 249–256. [[CrossRef](#)]
18. Olsson, W.A. The compressive strength of tuff as a function of strain rate from 10¹ to 10³/sec. *Int. J. Rock Mech. Min. Geomech. Abstr.* **1991**, *28*, 115–118. [[CrossRef](#)]
19. Zhang, Q.B.; Zhao, J. A Review of Dynamic Experimental Techniques and Mechanical Behaviour of Rock Materials. *Rock Mech. Rock Eng.* **2014**, *47*, 1411–1478. [[CrossRef](#)]
20. Feng, G.; Tang, L.; Zhou, K.; Ke, B. Mechanism Analysis of Liquid Carbon Dioxide Phase Transition for Fracturing Rock Masses. *Energies* **2018**, *11*, 2909.
21. Zhang, Y.; Deng, J.; Deng, H.; Ke, B. Peridynamics simulation of rock fracturing under liquid carbon dioxide blasting. *Int. J. Damage Mech.* **2018**, *28*, 1038–1052. [[CrossRef](#)]
22. Kuan, Z.; Dongwang, Z.; Guisong, Z. Performance research and application of carbon dioxide expansion blasting one-time cracking pipe. *Blasting* **2022**, *39*, 133–139.
23. Li, Q.Y.; Chen, G.; Luo, D.Y.; Ma, H.P.; Liu, Y. An experimental study of a novel liquid carbon dioxide rock-breaking technology. *Intern. J. Rock Mech. Min. Sci.* **2020**, *128*, 104244. [[CrossRef](#)]
24. Zhiliang, L. *Experiment Course on Rock Mechanics*; Chemical Industry Press: Beijing, China, 2010.
25. Qingxiang, D.; Zhaofeng, W.; Yabei, H. Research on TNT equivalent of liquid CO₂ phase-transition fracturing. *China Saf. Sci. J.* **2014**, *24*, 84–88.
26. Chaogui, M. *Study on the Influencing Factors and Parameter Optimization of Coal Body Caused by Carbon Dioxide Phase Change Blasting*; China University of Mining and Technology: Xuzhou, China, 2020.
27. Mingyu, W. *Study on Crack Propagation Law of Liquid Carbon Dioxide Phase Transition Blasting and Its Application*; China University of Mining and Technology: Xuzhou, China, 2018.
28. Yu, C.; Yue, H.; Li, H.; Xia, X.; Liu, B. Scale model test study of influence of joints on blasting vibration attenuation. *Bull. Eng. Geol. Environ.* **2021**, *80*, 533–550. [[CrossRef](#)]
29. Yu, C.; Yue, H.; Li, H.; Zuo, H.; Deng, S.; Liu, B. Study on the attenuation parameters of blasting vibration velocity in jointed rock masses. *Bull. Eng. Geol. Environ.* **2019**, *78*, 5357–5368. [[CrossRef](#)]

Disclaimer/Publisher's Note: The statements, opinions and data contained in all publications are solely those of the individual author(s) and contributor(s) and not of MDPI and/or the editor(s). MDPI and/or the editor(s) disclaim responsibility for any injury to people or property resulting from any ideas, methods, instructions or products referred to in the content.